The Astrophysical Journal, 588:1110–1120, 2003 May 10
© 2003. The American Astronomical Society. All rights reserved. Printed in U.S.A.

THE GEOMETRY OF RESONANT SIGNATURES IN DEBRIS DISKS WITH PLANETS

Marc J. Kuchner[1] and Matthew J. Holman
Harvard-Smithsonian Center for Astrophysics, 60 Garden Street, Cambridge, MA 02138;
mkuchner@cfa.harvard.edu, mholman@cfa.harvard.edu
Received 2002 September 9; accepted 2003 January 20

ABSTRACT

Using simple geometrical arguments, we paint an overview of the variety of resonant structures a single planet with moderate eccentricity ($e \lesssim 0.6$) can create in a dynamically cold, optically thin dust disk. This overview may serve as a key for interpreting images of perturbed debris disks and inferring the dynamical properties of the planets responsible for the perturbations. We compare the resonant geometries found in the solar system dust cloud with observations of dust clouds around Vega, ϵ Eridani, and Fomalhaut.

Subject headings: celestial mechanics — circumstellar matter — interplanetary medium — planetary systems — stars: individual (α Lyrae, ϵ Eridani, Fomalhaut)

1. INTRODUCTION

Direct imaging of nearby stars cannot yet detect light from extrasolar planets. However, imaging can detect circumstellar dust, and when a planet orbits inside a dust cloud, the planet can reshape the cloud dynamically, as Earth perturbs the solar dust cloud. Several debris disks around nearby main-sequence stars show structures and asymmetries that have been ascribed to planetary perturbations (Burrows et al. 1995; Holland et al. 1998, 2003; Schneider et al. 1999; Koerner, Sargent, & Ostroff 2001); perhaps these perturbed disks are signposts of extrasolar planetary systems.

Many of these disk features can be modeled as dust trapped in mean motion resonances (MMRs) with a planet. Gold (1975) suggested that as interplanetary dust spirals into the Sun under the influence of Poynting-Robertson (P-R) drag, planets could temporarily trap the dust in MMRs, creating ringlike density enhancements in the interplanetary cloud. Since then, both the *Infrared Astronomical Satellite* (*IRAS*) and the Diffuse Infrared Background Experiment (DIRBE) on the *Cosmic Background Explorer* (*COBE*) satellite have provided evidence for a ring of dust particles trapped by Earth (Jackson & Zook 1989; Reach 1991; Marzari & Vanzani 1994; Dermott et al. 1994; Reach et al. 1995). Models of Kuiper belt dust dynamics (Liou & Zook 1999) suggest that Neptune may also trap dust in first-order MMRs.

Other stars may host planets like Earth or Neptune. However, most of the known extrasolar planets do not resemble Earth or Neptune: they have masses in the range of $0.3M_J$–$15M_J$, and they often have significant orbital eccentricities (see, e.g., the review by Marcy & Butler 2000). Simulations by Kuchner & Holman (2001) show that planets as massive as these on eccentric orbits placed in a cloud of in-spiraling dust often create two concentrations of dust placed asymmetrically with respect to the star. Maps of the vicinity of Vega made with the IRAM Plateau de Bure interferometer at 1.3 mm (Wilner et al. 2002) and with the JCMT at 850 μm (Holland et al. 1998) reveal two concentrations of circumstellar emission whose asymmetries can be naturally explained by such a model, possibly indicating the presence of a few Jupiter mass planet in an eccentric orbit around Vega (Wilner et al. 2002). Other papers have numerically explored the interactions of particular planetary system configurations with a dust disk, with a view toward developing a general key for interpreting disk structures (Roques et al. 1994; Lecavelier Des Etangs et al. 1996; Liou & Zook 1999; Quillen & Thorndike 2002).

We assemble a primitive version of such a key by mapping the geometries of the MMRs that are likely to trap the most dust near a planet embedded in a debris disk. We illustrate the patterns formed by the libration centers of the trapped particles in an inertial frame—the frame of a distant observer. These basic patterns allow us to characterize four structures that probably span the range of high-contrast resonant structures a planet on an orbit with eccentricity up to $\sim$0.6 and low inclination can create in a dust disk.

Figure 1 shows these structures here for reference; we discuss them throughout the paper, particularly in § 4. Cases I and II in this figure represent the structures formed by planets on low-eccentricity orbits. Cases III and IV represent structures created by planets on moderately eccentric orbits. Cases I and III represent structures created by planets with substantially less than 0.1% of the mass of the star; cases II and IV represent structures created by more massive planets.

2. PLANETS ON LOW-ECCENTRICITY ORBITS

2.1. *Low-Mass Planets*

First, we review some of the physics of resonant dust rings created by relatively low mass planets, like Earth and Neptune. In the rest of this paper, we generalize the discussion to planets with mass up to $\sim 15M_J$ and e_0 up to $\sim$0.6. The resonant geometries we will describe apply to the general restricted three-body problem. However, we have in mind a source of dust, like the asteroid belt or the Kuiper belt, which releases dust on low-eccentricity orbits at semimajor axes, $a > a_0$, where a is the semimajor axis of the particle's orbit and a_0 is the semimajor axis of the planet's orbit. We use the convention that quantities with a subscript 0 refer to the planet.

[1] Michelson Postdoctoral Fellow.

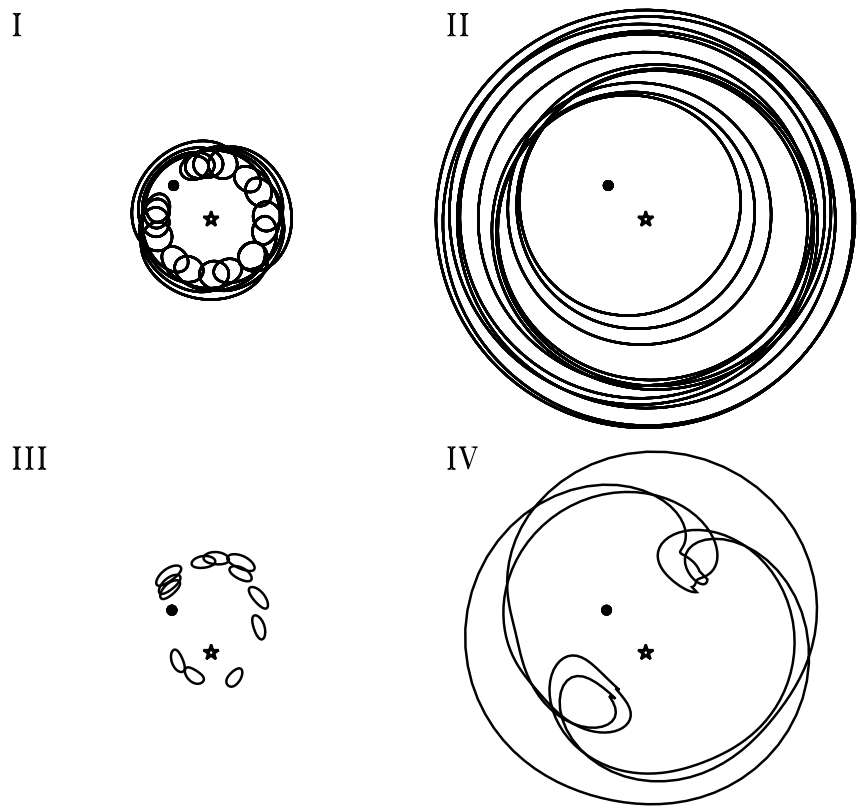

FIG. 1.—Four basic resonant structures: (I) low-mass planet on a low-eccentricity orbit, (II) high-mass planet on a low-eccentricity orbit, (III) low-mass planet on a moderate-eccentricity orbit, and (IV) high-mass planet on a moderate-eccentricity orbit.

We do not consider interactions between the dust grains, or between dust and any gas in the disk. For example, our approach does not apply to the gaseous, optically thick disks found around young stellar objects. However, the resonances we describe must underlie the basic resonant features of the solar system dust complex and debris disks around main-sequence stars with less than a few lunar masses of dust.

The radiation forces on a particle are parametrized by β, the strength of the stellar radiation pressure force on a particle divided by the strength of the stellar gravitational force on a particle. For a spherical particle with radius $s \gtrsim 1$ μm and density 2 g cm^{-3} orbiting a star with mass M_* and luminosity L_*,

$$\beta = \left(\frac{0.285\ \mu\text{m}}{s}\right)\left(\frac{L_*}{L_\odot}\right)\left(\frac{M_\odot}{M_*}\right) . \tag{1}$$

A typical particle in the solar system may have $s \approx 1$–100 μm (Grun et al. 1985; Fixsen & Dwek 2002), or $\beta \approx 0.285$–0.00285. Dust grains released at circumstellar distance r that are too large to be ejected by radiation pressure ($\beta \lesssim 0.5$) spiral into the star via P-R drag (Robertson 1937; Burns, Lamy, & Soter 1979), on a timescale

$$T_{\text{PR}} = \frac{400}{\beta}\left(\frac{M_\odot}{M_*}\right)\left(\frac{r}{1\ \text{AU}}\right)^2 \text{yr} . \tag{2}$$

Other drag forces, like solar wind, may also contribute to the decay of the particle's orbit (Banaszkiewicz, Fahr, & Scherer 1994).

Dust spiraling inward toward a planet encounters a series of exterior MMRs, each of which is associated with terms in the disturbing function of the form

$$\langle R \rangle_{\text{res}} = \frac{Gm_0}{a} F(\alpha, e, e_0) \cos\phi , \tag{3}$$

where G is the gravitational constant, m_0 is the mass of the planet, and $\alpha = a_0/a$ (see, e.g., Brouwer & Clemence 1961; Murray & Dermott 1999). The resonant argument, ϕ, is a linear combination of the orbital elements of the particle and the planet, which can be interpreted as an angle (Greenberg 1978). We do not discuss interior MMRs because they cannot sustain long-term trapping (see, e.g., Murray & Dermott 1999, p. 381). The potential, $\langle R \rangle_{\text{res}}$, causes the argument ϕ to accelerate. For a particle trapped in the resonance, ϕ librates about $\phi \approx 0$ if $F(\alpha, e, e_0) < 0$ and about $\phi \approx \pi$ if $F(\alpha, e, e_0) > 0$. An MMR of the form $j:k$ is nominally located at a semimajor axis given by $1/\alpha \approx (j/k)^{2/3}(1-\beta)^{1/3}$.

As a particle approaches the planet from afar, it encounters stronger and stronger resonances and has a better and better chance of becoming trapped. For particles approaching Earth or Neptune, the first resonances that are strong enough to trap substantial amounts of dust are the first-order MMRs: resonances of the form 2 : 1, 3 : 2, 4 : 3, etc. To first order in eccentricity and inclination, these resonances consist of pairs of terms with arguments

$$\phi_1 = j\lambda - (j-1)\lambda_0 - \varpi \tag{4a}$$

$$\phi_2 = j\lambda - (j-1)\lambda_0 - \varpi_0 , \tag{4b}$$

where λ and λ_0 are the mean longitudes of the particle and the planet and ϖ and ϖ_0 are the longitudes of pericenter of the particle and the planet, respectively. For Earth ($e_0 = 0.017$) and Neptune ($e_0 = 0.0086$), the ϕ_1 resonance dominates at all values of ϖ if the dust particle has even a small orbital eccentricity, and ϕ_1 librates about $\phi_1 \approx \pi$. Passage through this resonance slowly raises the particle's eccentricity, which asymptotically approaches a limiting value, $e_{\max}$, when the dynamics is followed using an expansion to second order in e (Weidenschilling & Jackson 1993; Sicardy et al. 1993; Beauge & Ferraz-Mello 1994; Liou & Zook 1997):

$$e_{\max} = \sqrt{\frac{2}{5j}} \, . \tag{5}$$

In the process, the particle's orbit becomes planet crossing, and in a matter of a few P-R times, the particle generally leaves the resonance via a close encounter with the planet (Marzari & Vanzani 1994) and an abrupt transition to a new orbit with a different eccentricity and semimajor axis. Near Earth, trapped dust populates several first-order MMRs.

The condition that ϕ_1 librates about $\phi_1 \approx \pi$ provides a relationship between λ and ϖ. Since rotations of the whole system by 2π must not affect the dynamics, we can write that the libration centers are located where

$$\lambda \approx \frac{(j-1)(\lambda_0 + 2\pi K) + \varpi + \pi}{j} \, , \quad \text{for } K \in \mathscr{Z} \, . \tag{6}$$

Figure 2 shows how this condition leads to the formation of a density wave, using the 3 : 2 MMR as an example. Figure 2*a* shows a variety of elliptical dust orbits, all with the same $1/\alpha = 1.31$ and $e = 0.8e_{\max}$, but with different ϖ-values. According to equation (6), each one of these orbits has $j = 3$ different longitudes that may be libration centers for a particle trapped in the ϕ_1 term. Figure 2*b* shows these three locations, marked with crosses, for each of two elliptical orbits with slightly different ϖ-values.

Figure 2*c* shows the locus of the libration centers for the whole range of elliptical orbits shown in Figure 2*a*. In Figure 2*d*, the planet has moved to a new longitude, and following equation (6), so have the libration centers. The density wave formed by the trapped particles resembles the pattern formed by the libration centers, blurred somewhat by

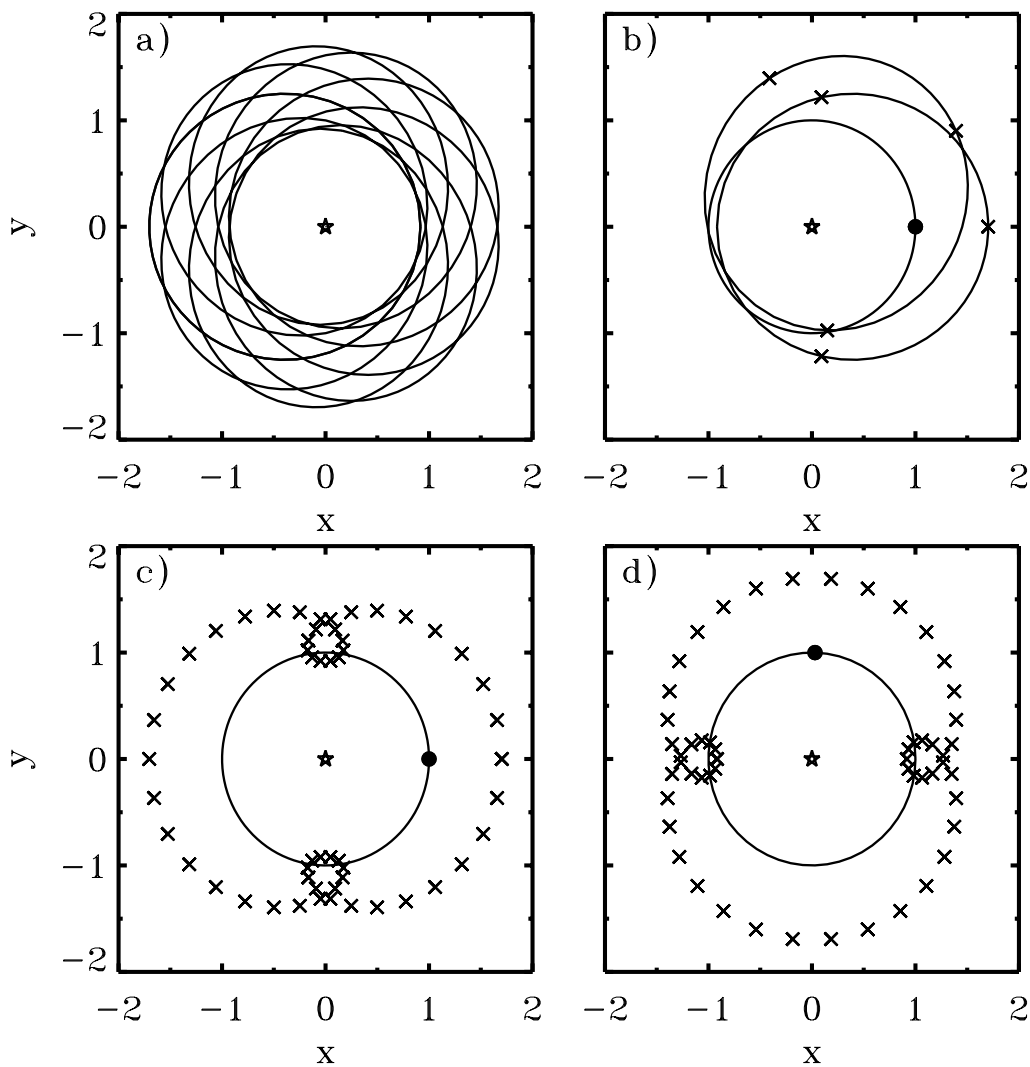

FIG. 2.—How a planet on a low-eccentricity orbit creates density waves. (*a*) Several particle orbits with different ϖ-values. (*b*) Libration centers of the $3j\lambda - 2\lambda_0 - \varpi$ term on two of these orbits, indicated by crosses. (*c*) Locus of all the libration centers. (*d*) Density wave appears to orbit at the same angular frequency as the planet (located at the filled circle).

libration, mostly in the azimuthal direction. Ozernoy et al. (2000) show some examples of how libration blurs the patterns formed by particles trapped in individual resonances.

Although any individual particle in Figure 2 moves steadily counterclockwise, slower than the planet, the density wave appears to rotate as a fixed pattern together with the planet. At conjunction ($\lambda = \lambda_0$) the resonance condition implies that $\varpi \approx \lambda_0 + \pi$, so the libration centers just outside the planet are always near apocenter. This condition creates the signature gap at the location of the planet seen in simulations of Earth's ring (Dermott et al. 1994) and of Kuiper belt dust interacting with Neptune (Liou & Zook 1999) and illustrated in Figure 1 (case I).

2.2. *Higher Mass Planets*

We can understand the range of possible resonant dust cloud structures by understanding the density wave patterns created by the series of MMRs that are likely to trap dust near a planet. Table 1 lists the arguments in a series of MMRs that figure most prominently in the sculpting of dust clouds (ignoring the planet's inclination, which first appears with order inclination squared) in order by α. It also lists the corresponding leading terms in $F(\alpha, e, e_0)$, evaluated for $\mu = 1/1047$ (i.e., Jupiter) and $\beta \ll 1$. The first MMRs in the list are the first-order resonances described above. For a given planet/dust cloud combination, a few MMRs generally dominate the observed resonant structure. In simulations of $\beta = 0.037$ dust particles approaching Earth (Dermott et al. 1994), the first-order $j = 4$–10 MMRs dominate the appearance of the trapped dust cloud. In simulations of Neptune's ring by Liou & Zook (1999), the 2 : 1 and 3 : 2 resonances ($j = 2$ and 3) dominate the appearance of the dust cloud.

The factor of Gm_0/a in equation (3) makes MMRs at large a weaker and less able to trap substantial quantities of dust. For more massive planets, however, the trapping probability for all MMRs is higher (Lazzaro et al. 1994), so particles approaching from afar become trapped sooner, in MMRs with longer orbital periods and larger semimajor axes. Likewise, close encounters with the planet more easily scatter dust grains out of exterior MMRs at small a, and this effect worsens with the mass of the planet.

The MMRs near the planet also become close together and begin to compete with one another. If $\mu = m_0/M_*$, the resonance overlap criterion (Wisdom 1980; Duncan, Quinn, & Tremaine 1989) predicts that first-order resonances with $j > 0.45[\mu(1-\beta)]^{-2/7} + 1$ are completely chaotic. This condition appears to place an absolute limit on how far down the chain of resonances a dust particle can be trapped. For large particles near Earth ($\mu \approx 3 \times 10^{-6}$), this criterion predicts that the first completely overlapped MMR is 17 : 18; for Neptune ($\mu \approx 5 \times 10^{-5}$) it is 8 : 9, and for Jupiter ($\mu \approx 10^{-3}$) it is 4 : 5.

As we have mentioned, many of the observed extrasolar planets have substantially more mass than planets in the solar system. Such massive planets quickly scatter dust from their first-order MMRs. Thus, after the first-order resonances, Table 1 lists the n : 1 resonances, the lowest order terms available at large semimajor axes—beyond the 2 : 1 MMR (nominally located at $a/a_0 = 1.59$). In numerical integrations, Kuchner & Holman (2001) and Wilner et al. (2002) found that dust spiraling inward toward a massive planet became trapped in this series of n : 1 resonances. Table 1 shows that the terms in these resonances that do not depend on the eccentricity of the planet have the form $j\lambda - \lambda_0 - (j-1)\varpi$. These terms must dominate when e_0 is small.

The $j\lambda - \lambda_0 - (j-1)\varpi$ terms in Table 1 are mostly positive, so most of these arguments librate around π. However, these terms all include contributions from indirect terms, which arise from the reflex motion of the star. The indirect contributions tend to reduce the strength of the resonance,

TABLE 1
RESONANT ARGUMENTS

Resonance	Nominal $1/\alpha$	$e_{\rm forced}/e_0$	Argument	Leading Term in $F(\alpha, e, e_0)$
6 : 5	1.13	0.96	$6\lambda - 5\lambda_0 - \varpi_0$	$-4.44181e_0$
			$6\lambda - 5\lambda_0 - \varpi$	$4.87053e$
5 : 4	1.16	0.94	$5\lambda - 4\lambda_0 - \varpi_0$	$-3.64001e_0$
			$5\lambda - 4\lambda_0 - \varpi$	$4.07424e$
4 : 3	1.21	0.92	$4\lambda - 3\lambda_0 - \varpi_0$	$-2.83462e_0$
			$4\lambda - 3\lambda_0 - \varpi$	$3.27756e$
3 : 2	1.31	0.87	$3\lambda - 2\lambda_0 - \varpi_0$	$-2.02226e_0$
			$3\lambda - 2\lambda_0 - \varpi$	$2.48115e$
2 : 1	1.59	0.74	$2\lambda - \lambda_0 - \varpi_0$	$-1.18945e_0$
			$2\lambda - \lambda_0 - \varpi$[a]	$0.426628e$
3 : 1	2.08	0.58	$3\lambda - \lambda_0 - 2\varpi_0$	$0.598757e_0^2$
			$3\lambda - \lambda_0 - \varpi_0 - \varpi$	$-2.21298e_0e$
			$3\lambda - \lambda_0 - 2\varpi$[a]	$-0.514804e^2$
4 : 1	2.52	0.49	$4\lambda - \lambda_0 - 3\varpi_0$	$-0.244422e_0^3$
			$4\lambda - \lambda_0 - 2\varpi_0 - \varpi$	$1.61636e_0^2e$
			$4\lambda - \lambda_0 - \varpi_0 - 2\varpi$	$-3.51697e_0e^2$
			$4\lambda - \lambda_0 - 3\varpi$[a]	$1.32796e^3$
5 : 1	2.92	0.42	$5\lambda - \lambda_0 - 4\varpi_0$	$0.0848968e_0^4$
			$5\lambda - \lambda_0 - 3\varpi_0 - \varpi$	$-0.855830e_0^3e$
			$5\lambda - \lambda_0 - 2\varpi_0 - 2\varpi$	$3.20820e_0^2e^2$
			$5\lambda - \lambda_0 - \varpi_0 - 3\varpi$	$-5.28443e_0e^3$
			$5\lambda - \lambda_0 - 4\varpi$[a]	$2.24457e^4$

[a] Includes contribution from indirect term.

and in the case of the 3 : 1, this effect makes the coefficient negative, so the $3\lambda - \lambda_0 - 2\varpi$ argument librates around 0.

The libration centers for the terms that librate around π are located at

$$\lambda \approx \frac{(j-1)\varpi + \lambda_0 + \pi(1+2K)}{j}, \quad \text{for } K \in \mathscr{Z}. \quad (7)$$

Again there are j libration centers spaced evenly around each elliptical dust orbit, and the locus of libration centers appears to corotate with the planet. This time, however, when we set $\lambda = \lambda_0$, we find that at conjunction, the particle can be in one of a few different places:

$$\varpi \approx \lambda_0 - \frac{\pi(1+2K)}{j-1} \quad \text{at conjunction}. \quad (8)$$

One can also show, following Weidenschilling & Jackson (1993), for example, that passage through a pure $j\lambda - \lambda_0 - (j-1)\varpi$ term raises the eccentricity of a dust particle in the same way that passage through a $j\lambda - (j-1)\lambda_0 - \varpi$ term does and that the limiting eccentricity is again given by equation (5). We can generate a rough picture of the density waves created by the dust trapped in these terms in the same manner as Figure 2, by drawing a variety of elliptical orbits with eccentricity $e \approx e_{\max}$ at an appropriate semimajor axis and using equation (7) (and Kepler's equation) to locate the libration centers on these orbits.

Figure 3 shows the patterns created by the most important resonant terms listed in Table 1. The first column of Figure 3 shows patterns for the terms that appear when the planet's eccentricity is low: the $j\lambda - (j-1)\lambda_0 - \varpi$ terms for first-order resonances and the $j\lambda - \lambda_0 - (j-1)\varpi$ terms for $n:1$ resonances. The patterns are the locii of the libration centers, generated in the manner of Figure 2.

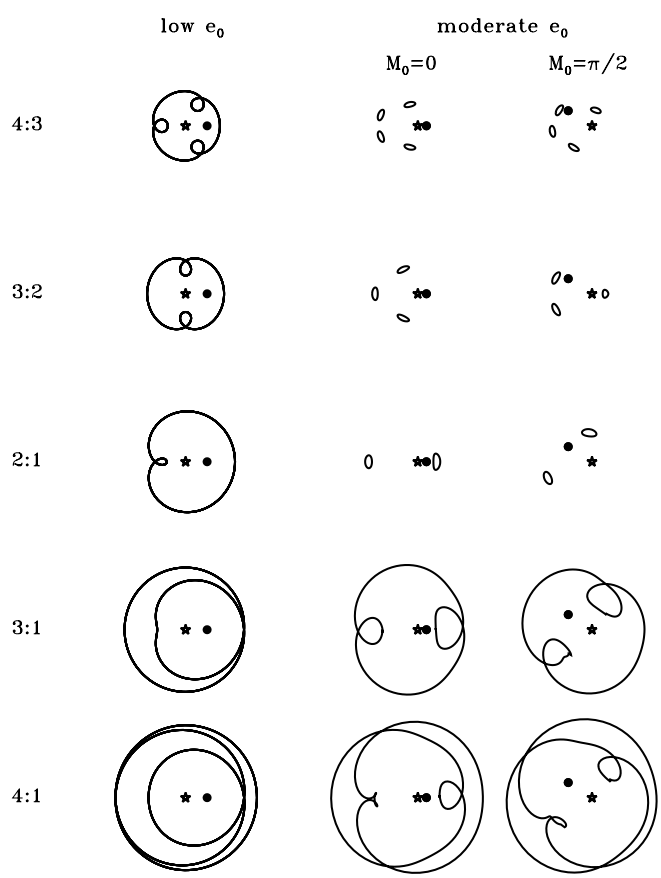

FIG. 3.—Patterns formed by dust in MMRs listed in Table 1

3. PLANETS ON ECCENTRIC ORBITS

The patterns in the first column of Figure 3 appear in Murray & Dermott (1999, p. 325), derived in a slightly different context—by tracing the path of a particle in a frame corotating with the planet. However, the literature offers little discussion of resonant structures created by planets on eccentric orbits, and this case is crucial for understanding extrasolar planetary systems. Naturally, for a planet on an eccentric orbit, there is no simple corotating frame. However, we can deduce the resonance patterns associated with planets on eccentric orbits by building on the arguments used above.

3.1. *Secular Effects*

Besides resonant perturbations, planets introduce secular perturbations to the orbits of nearby particles. When the planet's orbit is eccentric, these perturbations generally produce a correlation between e and ϖ. We must consider these effects when we examine MMRs with planets on eccentric orbits.

We can demonstrate the importance of secular perturbations by comparing them with radiation forces. Near a planet, the P-R time, and thereby the trapping time, is longer than the secular timescale for dust grains with $\beta < \beta_0$, where

$$\beta_0 = 100\left(\frac{M_*}{M_\odot}\right)^{-1/2}\left(\frac{a}{1\ \text{AU}}\right)^{1/2} \alpha b^1_{3/2}(\alpha)\mu, \quad (9)$$

and the Laplace coefficient (size order unity) is

$$b^m_{3/2}(\alpha) = \frac{1}{\pi}\int_0^{2\pi} \frac{\cos m\psi\, d\psi}{(1 - 2\alpha\cos\psi + \alpha^2)^{3/2}}, \quad (10)$$

i.e., $\beta_0 \sim 100\mu$. For example, $\beta_0 = 0.022$ for Neptune, while $\beta_0 = 0.44$ for a Jupiter mass planet orbiting Vega at $a = 40$ AU. Thus, we can expect most observable particles in the cases we are interested in ($10^{-5} \lesssim \mu \lesssim 10^{-2}$) to suffer significant secular evolution while they are trapped in an MMR. Secular perturbations from planets with eccentric orbits affect all dust particles in their vicinity, even those that are not in strong MMRs.

In the Laplace-Lagrange description of secular perturbations, valid for $e, e_0 \ll 1$, a particle's osculating e and ϖ are expressed as a combination of constant forced elements, e_{forced} and ϖ_{forced}, and time-varying free elements, e_{free} and ϖ_{free}. Secular evolution is easily visualized in the (h, k) coordinate system, where $h = e\cos\varpi$ and $k = e\sin\varpi$. In this system, we write $h = h_{\text{forced}} + h_{\text{free}}$ and $k = k_{\text{forced}} + k_{\text{free}}$.

When there is only a single perturbing planet on a fixed orbit, the particle's forced elements are constant, and the osculating elements, h and k, trace out a circle centered on $(h_{\text{forced}}, k_{\text{forced}})$ with a radius of e_{free}. The forced longitude of pericenter is $\varpi_{\text{forced}} = \arctan(k_{\text{forced}}/h_{\text{forced}}) = \varpi_0$, and the forced eccentricity is

$$e_{\text{forced}} = \sqrt{h^2_{\text{forced}} + k^2_{\text{forced}}} = \frac{b^2_{3/2}(\alpha)}{b^1_{3/2}(\alpha)} e_0. \quad (11)$$

As a approaches a_0, $e_{\rm forced}$ approaches e_0. Table 1 lists the approximate value of $e_{\rm forced}/e_0$ at the nominal α for each MMR.

In a cloud of many particles, many orbits with a range of $h_{\rm free}$ and $k_{\rm free}$ are occupied. However, all particles with a given semimajor axis will have the same $h_{\rm forced}$ and $k_{\rm forced}$. For example, if all particles are released on circular orbits outside the planet's orbit and outside of any MMRs, then the Laplace-Lagrange solution prescribes that at any given time all the particles with a given semimajor axis will occupy a circle with radius $e_{\rm free}$ centered on the point ($h_{\rm forced}$, $k_{\rm forced}$) in the (h, k)-plane. Dermott et al. (1985) and Wyatt et al. (1999) showed that a set of orbits occupying such a circle in the (h, k)-plane form a cloud that is roughly circular, but the center of the cloud is offset from the star a distance $e_0 a_0$ along the planet's apsidal line in the direction of the center of the planet's orbit. Hence, the background dust cloud in the vicinity of a large planet should often appear circular in the absence of MMRs, although if the planet's orbit is eccentric, the center of the circle will be offset from the star.

When the perturber has higher eccentricity, or when a particle is in an MMR, the particle's secular trajectory changes somewhat: the orbit no longer traces an exact circle in the (h, k)-plane, even when the librations are averaged away (Wisdom 1983). However, the character of the averaged secular motion often remains the same: h and k follow a simple closed loop around ($h_{\rm forced}$, $k_{\rm forced}$). We will retain the spirit of the Laplace-Lagrange approximation for the secular motion of the particles for the remainder of this paper, and we will refer loosely to free and forced elements, even when we are discussing resonant orbits. We find that this approximation suffices for our broad exploration of planetary signatures in debris disks.

3.2. *Mean Motion Resonances*

When a particle is trapped in an MMR with a planet on a circular orbit, the resonant argument that only depends on ϖ, not on ϖ_0, dominates the particle's motion. The other terms in the resonance have coefficients $F(e, e_0)$ that are zero when e_0 is zero. However, when a particle is trapped in an MMR with a planet on an eccentric orbit, resonant arguments that depend on ϖ_0 may come into play.

To leading order, the averaged disturbing function for an MMR with a planet on an eccentric orbit is the sum of two or more terms:

$$\langle R\rangle_{\rm res} = \frac{Gm_0}{a}\sum_{\xi} F_\xi(\alpha, e, e_0)\cos\phi_\xi\ , \tag{12}$$

where, as Table 1 shows, $\phi_1 = p\lambda - q\lambda_0 + (p-q)\varpi$ and $\phi_\xi = \phi_1 + (\xi - 1)(\varpi - \varpi_0)$. Following Wisdom (1983), we can reexpress this sum as

$$\langle R\rangle_{\rm res} = \frac{Gm_0}{a} F'(\alpha, e, e_0, \varpi, \varpi_0)\cos\phi'\ , \tag{13}$$

where

$$\phi' = \phi_1 + \arctan\left\{\frac{\sum_{\xi=2}^{p}|F_\xi|\sin\left[(\xi-1)(\varpi-\varpi_0)+\delta_\xi\right]}{|F_\xi| + \sum_{\xi=2}^{p}|F_\xi|\cos\left[(\xi-1)(\varpi-\varpi_0)+\delta_\xi\right]}\right\} \tag{14}$$

and

$$F'(\alpha, e, e_0, \varpi, \varpi_0) = \left\{\left[\sum_{\xi} F_\xi(\alpha, e, e_0)\sin\phi_\xi\right]^2 + \left[\sum_{\xi} F_\xi(\alpha, e, e_0)\cos\phi_\xi\right]^2\right\}^{1/2}\ . \tag{15}$$

The quantity $\delta_\xi = \pi$ for $F_\xi < 0$ and $\delta_\xi = 0$ otherwise. We define F' to be always ≥ 0, so on resonance, the new argument, ϕ', librates around $\phi' \approx \pi$. Equation (14) shows explicitly that the differences among the terms only appear on a secular timescale, as $\varpi - \varpi_0$ precesses.

At any moment, the particle's orbit may be viewed as undergoing libration about $\phi' = \pi$. This change in the effective resonant argument can change the constraints on the orbital elements of resonant objects, which can result in dramatically different looking clouds of trapped particles. Often one term dominates, in the sense that $\phi' \approx \phi_\xi$ or $\phi' \approx \phi_\xi + \pi$. This circumstance depends on e, e_0, ϖ, ϖ_0, and the details of trapping, but we can appeal to numerical simulations and use what we know about the secular evolution of dust particles to help decide which terms are likely to be most important.

3.3. *High-Mass Planets*

It is easier to consider high-mass planets first because the $n:1$ resonances that dominate the appearance of dust clouds containing a massive planet are farther from the planet than the first-order resonances that dominate in the case of a low-mass planet. Particles released on circular orbits approach a planet with $e_{\rm free} \approx e_{\rm forced}$, so they reach the $n:1$ MMRs with e ranging from 0 to $e_{\rm forced} + e_{\rm free}$. As Table 1 shows, $e_{\rm forced} \approx e_0/2$ near the lowest order $n:1$ MMRs. When $\varpi \approx \varpi_0 + \pi$, all the terms become degenerate, in the sense that all of their libration centers occur at the same longitudes. At the other end of the range of secular motion, $\varpi \approx \varpi_0$ and $e \approx e_0$, so according to equation (14), the term with the largest coefficient in $F(\alpha, e, e_0)$ will dominate the motion of the particles.

The arguments that match the terms with the largest coefficients in $F(\alpha, e, e_0)$ (see Table 1) share a second common form: $j\lambda - \lambda_0 - \varpi_0 - (j-2)\varpi$. Numerical integrations (Wilner et al. 2002) confirm that these terms dominate the resonant dynamics over a wide range of planet eccentricities. These terms always have $F(\alpha, e, e_0) < 0$, so the corresponding arguments librate about 0. The j libration centers on each ellipse are located at

$$\lambda \approx \frac{\lambda_0 + \varpi_0 + (j-2)\varpi + 2\pi K}{j}\ , \quad \text{for } K \in \mathscr{Z}\ . \tag{16}$$

We reserve a discussion of the complicated secular dynamics of these resonances for a future paper.

Figure 4 illustrates the pattern formed by particles in the $3\lambda - \lambda_0 - \varpi_0 - \varpi$ term near a planet with $e_0 = 0.6$. Once a particle is trapped in resonance, its secular evolution no longer obeys the Laplace-Lagrange solution, but the libration centers of the trapped particles will still occupy a closed curve in the (h, k)-plane. Figure 4*a* shows such a variety of orbits centered on $h = 0.58e_0$, $k = 0$. Orbits that are close to apse alignment with the planet have higher eccentricities. Like the Laplace-Lagrange orbit distributions discussed by

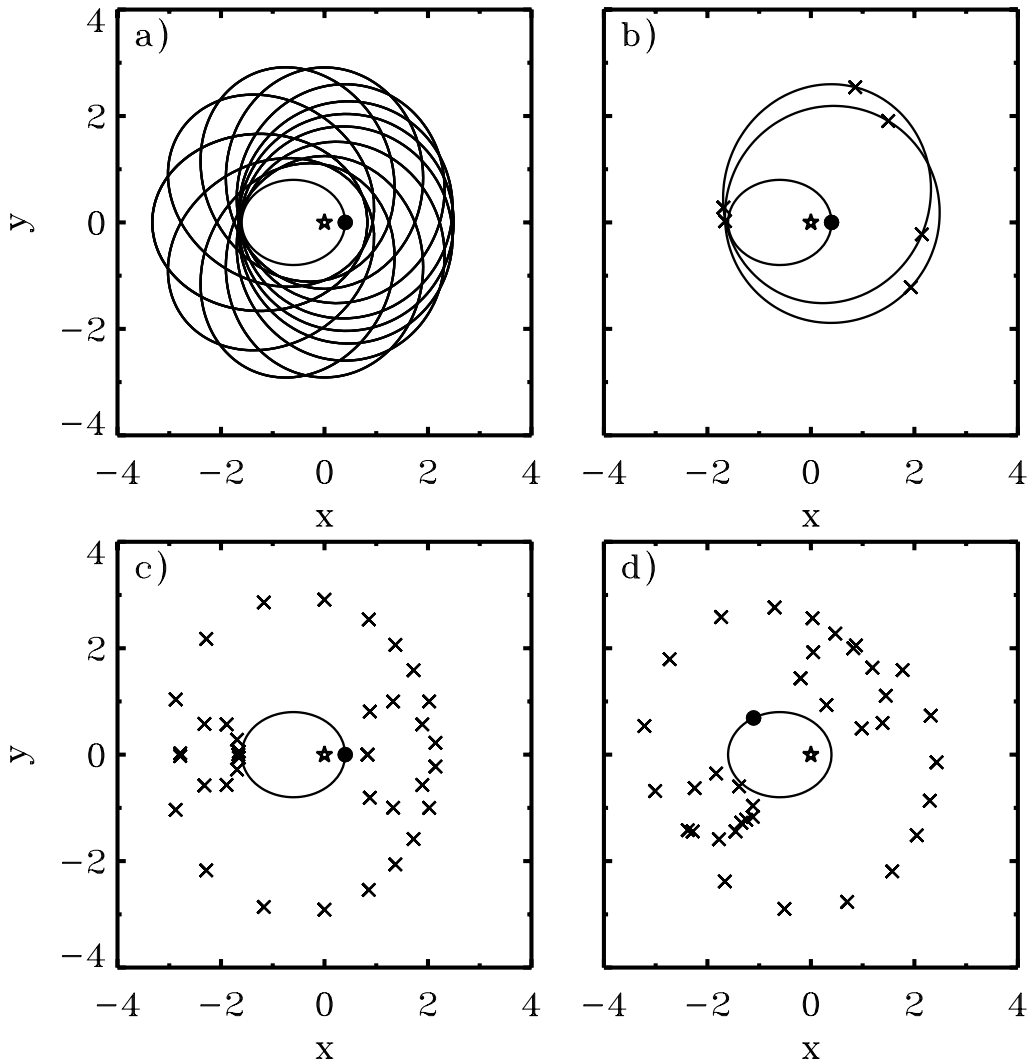

FIG. 4.—Libration centers of the $3\lambda - \lambda_0 - \varpi_0 - \varpi$ term. (*a*) Several particle orbits with different e and ϖ. (*b*) The libration centers on two of these orbits when the planet is at pericenter. (*c*) All the libration centers. (*d*) Clumps formed by particles trapped in this term appear to rotate at half the angular frequency of the planet.

Dermott et al. (1985) and Wyatt et al. (1999), these orbits taken together form a pattern that is roughly circular, but the center of the circle is offset from the star along the planet's apsidal line in the direction of the center of the planet's orbit.

Figure 4*b* shows the three libration centers on two of these orbits, calculated from equation (16). By definition, $\lambda = M + \varpi$, where M is the particle's mean anomaly. For particles at pericenter, $M = 0$ and $\lambda = \varpi$, so for particles trapped in *any* $j\lambda - \lambda_0 - \varpi_0 - (j-2)\varpi$ term,

$$\varpi \approx \frac{M_0}{2} + \varpi_0 + \pi K\ , \quad \text{for } K \in \mathscr{Z}\ , \tag{17}$$

where M_0 is the planet's mean anomaly. In other words, the libration centers for this family of terms reach pericenter at two different longitudes, and these special longitudes precess at an angular frequency equal to half the Keplerian angular frequency of the planet. When the planet reaches pericenter ($M_0 = 0$), so do the particles on orbits that are apse aligned or anti–apse aligned with the planet's orbit. Figures 4*c* and 4*d* show that the locus of libration centers makes a characteristic two-lobed pattern, which appears to rotate at half the mean angular frequency of the planet. The center of this apparent rotation lies on the planet's apsidal line between the star and the center of the planet's orbit.

3.4. *Low-Mass Planets*

The resonances populated near low-mass planets cluster at semimajor axes near the planet's semimajor axis, where $e_{\rm forced} \approx e_0$. In this vicinity, the resonant orbits can easily become planet crossing unless they are roughly apse aligned with the planet's orbit, i.e., $e_{\rm free} < e_{\rm forced}$ and $\varpi \approx \varpi_0$. Figure 5*a* shows a collection of roughly apse-aligned orbits, all with $e_{\rm forced} = 0.5$ and $e_{\rm free} = 0.12$. In the absence of MMRs, the combination of these elliptical orbits would appear as an elliptical ring.

For the case of the 3 : 2 MMR, a single one of these orbits has three libration centers, shown in Figure 5*b*. For a family of orbits that must remain roughly apse aligned with the planet, the secular spread in the libration centers is necessarily small, and the resonant arguments are all roughly equal. Hence, as Figure 5*c* shows, we should expect the density wave to resemble the pattern produced by the libration centers in any one orbit; the libration centers associated with

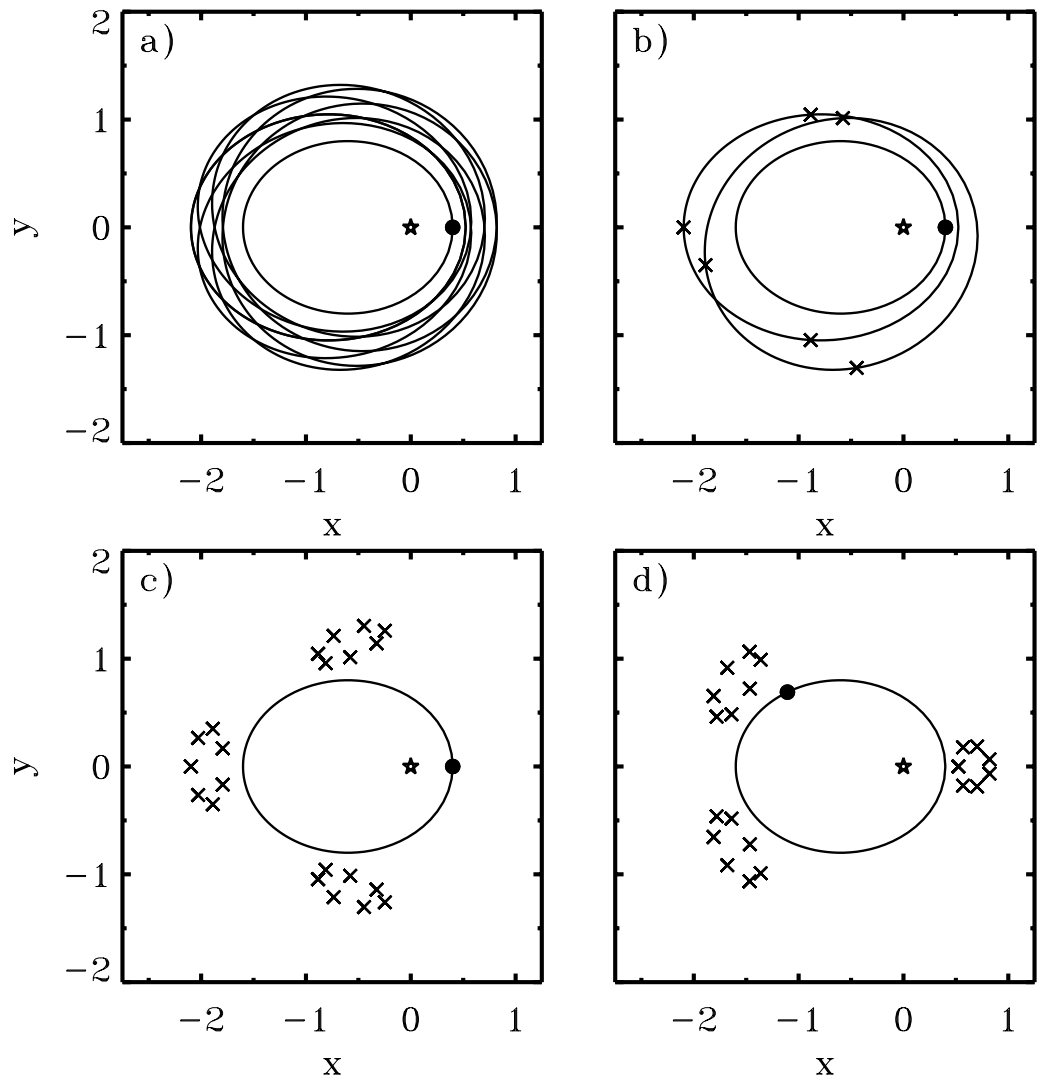

FIG. 5.—How dust confined to the 3 : 2 MMR near a planet on a moderately eccentric orbit might appear. (*a*) Several orbits with different e and ϖ, distributed in a Laplace-Lagrange circle with small $e_{\rm free}$. (*b*) Libration centers on two of these orbits when the planet is at pericenter. (*c*) All the libration centers. (*d*) Three dust clumps really do orbit at $\frac{2}{3}$ of the planet's orbital frequency.

any MMR of the form $j:k$ form a set of j clumps. As Figure 5*d* shows, the locus of all the libration centers orbits at k/j times the angular frequency of the planet; when the planet's mean anomaly changes by $\pi/2$, the mean anomalies of the clumps of particles in the 3 : 2 MMR change by $\pi/3$.

An exterior first-order MMR has two relevant terms (eqs. [4a] and [4b]), and for the second term, $F_2(\alpha, e, e_0) < 0$. For this case, equation (15) becomes

$$\phi' = \phi_1 + \arctan\left[\frac{|F_2(\alpha, e, e_0)|\sin(\varpi - \varpi_0 + \pi)}{|F_1(\alpha, e, e_0)| + |F_2(\alpha, e, e_0)|\cos(\varpi - \varpi_0 + \pi)}\right]. \tag{18}$$

A key difference between the two terms is that one argument librates around 0, the other around π.

Deciding which resonances dominate in the vicinity of a low-mass planet on an eccentric orbit can be tricky. When $|F_1(\alpha, e, e_0)| \gg |F_2(\alpha, e, e_0)|$, $\phi' \approx \phi_1$. When $|F_1(\alpha, e, e_0)| \ll |F_2(\alpha, e, e_0)|$, $\phi' \approx \phi_2 + \pi$. However, when $F_1(\alpha, e, e_0) \approx F_2(\alpha, e, e_0)$, the two terms tend to cancel each other, that is, $|F'| \approx |F_1 - F_2|$ when $\varpi \approx \varpi_0$. This cancellation diminishes the strength of the resonance.

Therefore, we should expect first-order resonances to be relatively weak for a dust particle whose orbit has been secularly apse aligned with the planet's orbit. At $e = e_{\rm forced}$, the ϕ_1 resonance generally has the larger coefficient. The 2 : 1 MMR is an exception because F_1 for the 2 : 1 is diminished by an indirect term, so the ϕ_2 resonance easily dominates. We leave it to numerical studies (Quillen & Thorndike 2002) to decide which MMRs and terms dominate in a given system containing a low-mass, high-eccentricity planet. However, no matter which MMRs dominate, we expect the same generic behavior: the trapped dust will form an eccentric ring of dust clumps.

4. PLANETARY SIGNATURES

4.1. *Four Basic Cloud Structures*

The first column of Figure 3 illustrates the density waves formed by the resonant terms we expect will dominate the

appearance of dust clouds near planets with low orbital eccentricity. The second and third columns illustrate the density waves formed by the resonant terms we expect will dominate near planets with moderate orbital eccentricity: the $j\lambda - (j-1)\lambda_0 - \varpi_0$ terms for first-order resonances and the $j\lambda - \lambda_0 - \varpi_0 - (j-2)\varpi$ terms for $n:1$ resonances. In the second column, the planet is at pericenter; in the third column, the planet is at $M_0 = \pi/2$.

Our map of these basic patterns prepares us to consider more generally the appearance of a dust disk in the vicinity of a planet, where trapped dust occupies several MMRs. Now we can describe the origin of the structures shown in Figure 1: they are superpositions of the patterns shown in Figure 3.

Cases I and II are superpositions of the patterns depicted in the left-hand column of Figure 3. Cases III and IV are superpositions of the patterns depicted in the right-hand column of Figure 3 (and also in the middle column, at a different planetary orbital phase). In general, the rings created by the low-eccentricity planets appear to corotate with the planet, but the resonant structures created by moderate-eccentricity planets do not because the density wave patterns associated with the resonances they excite vary with the planet's orbital phase. The cases are as follows:

1. Case I: a low-mass planet with low orbital eccentricity, like Earth or Neptune, traps dust in first-order $j\lambda - (j-1)\lambda_0 - \varpi$ resonances. Case I shows a superposition of patterns produced by terms of this form, the patterns in the upper left-hand column of Figure 3. Populating these resonances creates a ring with a gap at the location of the planet.
2. Case II: a higher mass planet on a low-eccentricity orbit traps dust in more distant $n:1$ resonances, in terms of the form $j\lambda - \lambda_0 - (j-1)\varpi$. Case II shows superpositions of patterns produced by such terms, the patterns in the lower left-hand column of Figure 3. These resonances create a larger ring with a smooth central hole.
3. Case III: a low-mass planet on a moderately eccentric orbit traps dust in MMRs with small secular motion near apse alignment with the planet, creating a blobby eccentric ring. The blobs in this ring appear to be continually created and destroyed, as dust clumps occupying different MMRs pass through one another. The more highly concentrated clumps are located near the apocenter of the planet's orbit, where all the particles in the $j\lambda - (j-1)\lambda_0 - \varpi_0$ terms (except for the $2:1$) are constrained to have their conjunctions. The planet may or may not be located near a gap in the ring.
4. Case IV: a high-mass planet on a moderately eccentric orbit creates a ring offset from the star containing a pair of clumps, where the two-lobed patterns of all the $n:1$ resonances of the form $j\lambda - \lambda_0 - (j-2)\varpi - \varpi_0$ coincide. The clumps appear to orbit a point along the planet's apsidal line, between the star and the planet, at half the mean orbital frequency of the planet.

Naturally, intermediate cases will result in more than one variety of resonance being populated by dust particles; these clouds can possess features of more than one of the extreme cases shown in Figure 1. For example, an intermediate-mass planet on a low-eccentricity orbit will have a slightly larger ring with a less prominent gap at the location of the planet than case I. A planet with intermediate eccentricity may have both a ring component and blobs, although librational motion may smear these blobs so that they blend into the ring.

4.2. *Strong Drag Forces: Wakes*

When the drag force is large and the planet's mass is small, the libration centers can shift substantially from π. For an MMR containing a collection of resonant arguments of the form $\phi = j\lambda - k\lambda_0 - (j-1)\varpi - (\xi - 1)(\varpi_0 - \varpi)$, the resonant perturbations are

$$\left[\frac{da}{dt}\right]_{\rm res} = -2jan\mu F'(\alpha, e, e_0, \varpi, \varpi_0)\sin\phi' , \quad (19)$$

$$\left[\frac{de}{dt}\right]_{\rm res} = -n\mu F'(\alpha, e, e_0, \varpi, \varpi_0)\sin\phi' , \quad (20)$$

where the particle's angular frequency, n, on resonance is nominally

$$n = \left[\frac{GM_*(1-\beta)}{a^3}\right]^{1/2} . \quad (21)$$

P-R drag causes relatively slow changes in a and e (Wyatt & Whipple 1950):

$$\left[\frac{da}{dt}\right]_{\rm PR} = \frac{-GM_*\beta}{ac}\frac{(2+3e^2)}{(1-e^2)^{3/2}} , \quad (22)$$

$$\left[\frac{de}{dt}\right]_{\rm PR} = \frac{-5GM_*\beta}{2a^2c}\frac{(2+3e^2)}{(1-e^2)^{1/2}} , \quad (23)$$

where c is the speed of light. To locate the libration centers, we set $[da/dt]_{\rm PR} + [da/dt]_{\rm PR} = 0$ and find

$$\sin\phi_0 = -\frac{(GM_*/a)^{1/2}\beta(1-\beta)}{2j\mu cF'(\alpha, e, e_0, \varpi, \varpi_0)}\frac{(2+3e^2)}{(1-e^2)^{3/2}} . \quad (24)$$

On resonance, ϕ' librates around ϕ_0, which is greater than π.

For the case of a planet on a circular orbit, the observable effect on a dust cloud is a shift in the locations of the pericenters of the orbits of the trapped particles. In the absence of this effect, the libration centers first reach pericenter at an angle π/k behind the planet. With this effect, the first pericenter is located closer to the planet, at an angle $(2\pi - \phi_0)/k$. This asymmetry concentrates the trapped dust from Earth's ring into a blob trailing Earth, sometimes called Earth's "wake" (Dermott et al. 1994; Reach et al. 1995).

Figure 6 shows an example of how cases I and III, as illustrated in Figure 1, could appear when the perturber's gravity is weak compared to the drag force and the shifts in the libration centers are substantial. Case I shows a wake trailing the planet. For the terms illustrated in the second and third columns of Figure 3, the shift in the libration center appears as a displacement of the density enhancements. The $n:1$ resonance clumps will appear at $\varpi = K\pi + M_0/2 + \varpi_0 + (\phi_0 - \pi)/2$; i.e., their longitudes shift by $(\phi_0 - \pi)/2$. The first-order resonance clumps near low-mass planets on moderately eccentric orbits (Case III) shift by $(\phi_0 - \pi)/k$ in the prograde direction.

This effect depends on the velocity of the dust [$\sim(GM_*/a)^{1/2}$], on β, and on the mass of the planet; it is more pronounced for small dust grains and low-mass planets close to massive and luminous stars. It is negligible for patterns generated by more massive planets (cases II and IV), even if the

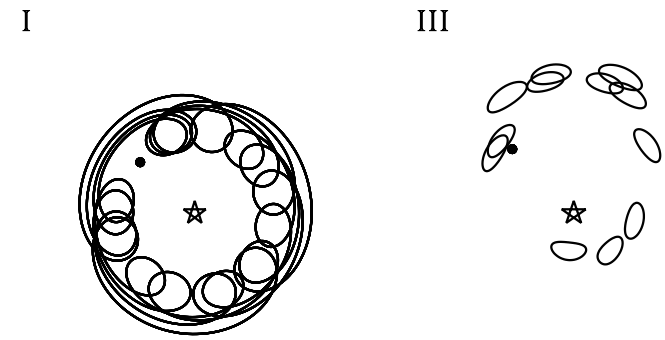

FIG. 6.—Cases I and III when the drag force is particularly strong and the planet's mass is small. Case I develops a "wake" trailing the planet. The blobs in Case III shift in the prograde direction.

planets are in 3 day orbits. Moreover, this effect does not appear in simulations of Neptune's ring (Liou & Zook 1999) since even Neptune has high mass (and low orbital velocity) compared to Earth. The ϵ Eridani ring seen by JCMT (Holland et al. 1998) probably does not show this effect either for the same reasons.

5. DISCUSSION

5.1. *Observed Examples*

Earth is the only planet in the solar system whose resonant ring has been detected (Kuchner, Reach, & Brown 2000). This wake in this ring produces an asymmetry in the thermal infrared background between the direction leading Earth and the direction trailing Earth, which *IRAS* and *COBE*/DIRBE detected (Reach 1991; Dermott et al. 1994; Reach et al. 1995). Indeed, Earth's ring is the only observed resonant dust cloud structure—in the solar system or elsewhere—identified with an independently observed planet! However, models of Kuiper belt dust interacting with the outer planets suggest that Neptune also creates a type I ring with a characteristic hole at the location of the planet.

Images of nearby stars with debris disks supply further examples of rings that point to undetected planets. Dust clouds around Vega, β Pictoris, ϵ Eridani, and Fomalhaut have all been imaged at submillimeter wavelengths (Holland et al. 1998, 2003; Greaves et al. 1998). The β Pictoris disk is edge-on, making its resonant rings hard to distinguish, if it has any. However, the other systems appear to contain resonant rings that may be easier to classify:

1. Vega: the Vega debris disk may provide an example of case IV. Submillimeter images of Vega (Wilner et al. 2002) show two concentrations of emission that resemble those in Figure 1; they are not colinear with the star, and one is closer to the star than the other. Wilner et al. (2002) used this model to estimate that the perturbing planet has mass $\mu \approx 10^{-3}$ and eccentricity $e \approx 0.6$ and used the locations of the two knots of emission to infer the planet's current location.

2. ϵ Eridani: case III may be a good model for the ϵ Eridani dust ring, which has roughly four major concentrations of emission irregularly placed around the ring and an apparent gap in the ring. As Figure 1 shows, the low-mass, moderate-eccentricity planet model naturally explains the presence of a few dust clumps of various concentrations. Quillen & Thorndike (2002) have developed a numerical model of type III for the ϵ Eridani dust ring using the numerical technique developed by Kuchner & Holman (2001). They find that dust released just outside a planet with eccentricity 0.3 and mass $\mu = 10^{-4}$ becomes trapped in the 5 : 3 and the 3 : 2 MMRs with the planet and forms a blobby eccentric ring like the one in Figure 1. The second order 5 : 3 MMR may be relatively strong because the first-order resonances suffer from the cancellation described in § 3.4. Although dust trapped in these resonances probably forms relatively narrow rings, the large beam of the JCMT could easily blur such a narrow blobby ring into something resembling the Holland et al. (1998) image, as Quillen & Thorndike (2002) illustrate.

3. Fomalhaut: the A3 V star Fomalhaut has a circumstellar dust cloud, recently identified as a ring with an azimuthal asymmetry representing $\sim$5% of the total flux from the disk (Holland et al. 2003). This ring is difficult to classify, since it is roughly 20° from edge-on. Wyatt & Dent (2002) suggest that the dust may be trapped in a 2 : 1 MMR with a planet, and Holland et al. (2003) suggest that the dust might be trapped in a 1 : 1 MMR with a planet. However, the 1 : 1 MMRs are much harder to populate with dust than the MMRs we consider here, and contrary to Ozernoy et al. (2000), we consider it improbable that a single MMR, even the 2 : 1, could dominate the appearance of a real dust cloud, particularly one as collisional as Fomalhaut's. More likely, the structure in the Fomalhaut ring arises from collisions (Wyatt & Dent 2002), or if resonant trapping is responsible for the azimuthal structure, there is another clump to be found, perhaps obscured by the limb brightening.

We know no observed examples of case II rings. However, the close-in extrasolar planets with periods less than $\sim$30 days have nearly circular orbits, probably as a result of tidal effects (Marcy & Butler 2000). Any dust disks associated with these planets could form examples of case II.

5.2. *Other Considerations*

We have only addressed the geometry of resonant dust orbits. A variety of other phenomena may affect the appearance of an actual debris disk. For example, we have not discussed how the resonances are populated. Different resonances may dominate when a disk is fed by a belt of asteroids or comets whose orbits are restricted to a small region of phase space.

Furthermore, many known dust disks are collisional. For systems like the rings of Saturn, where each particle has a collision roughly once per orbit, the collisions dominate the resonant effects we catalog here, and a fluid description of the particles becomes more appropriate. Collisions that occur on intermediate timescales, however, may leave particles trammeled in the net of the underlying strong resonances, altering only the spectrum of populated MMRs. For example, mutual collisions among dust grains may destroy dust particles before they can access all the strong resonances; this effect would preserve the basic four structures shown in Figure 1.

We have also neglected the terms in MMRs that depend on the inclinations and restricted our analysis to planets with moderate eccentricity. At high planet inclinations ($i^2 \sim 1$) and eccentricities ($e^2 \sim 1$), many new terms in the disturbing function become relevant. These effects can alter the basic resonant geometries.

Many planetary systems have more than one planet; we have also only considered the effects of one planet. Since we are only interested in high-contrast structures, we may justify this approach by saying that we only care about the first massive planet to encounter the in-spiraling dust, that is, massive enough to create a high-contrast structure by ejecting most of the dust grains as they pass. For example, in simulations by Liou & Zook (1999), Neptune ejects most of the in-spiraling Kuiper belt particles before they can encounter any other planets; we are interested in analogous planets. However, the secular evolution of a multiple-planet system may affect how a planet interacts with a dust cloud, even if little dust reaches most of the planets, and they do not carve their own signatures.

Finally, we have tacitly assumed that the dust cloud is observed face-on. Disks that are tilted from face-on may show a variety of asymmetries due to effects other than resonant trapping, such as the *IRAS*/DIRBE dust bands (Hauser et al. 1984), secular warps (Augereau et al. 2001), and limb brightening.

6. CONCLUSIONS

Four basic structures probably represent the range of high-contrast resonant structures a planet with eccentricity $\lesssim 0.6$ can create in a disk of dust released on low-eccentricity orbits: a ring with a gap at the location of the planet, a smooth ring, a blobby eccentric ring, and an offset ring plus a pair of clumps. Some of these structures have slowly become revealed in numerical simulations of particular debris disks; we have chased them to their dens in the resonant landscape of the three-body problem. The crude key we have assembled should help classify the debris disk structures seen by upcoming telescopes like *SIRTF*, SOFIA, ALMA, *JWST*, and Darwin/*TPF*.

Observing one of these structures instantaneously should allow us to categorize the planet as high or low mass (compared to Jupiter orbiting the Sun) and low or moderate eccentricity (compared to $e_0 \sim 0.2$). In the case of a ring with a gap or an offset ring plus a pair of clumps, the image of the face-on cloud directly indicates the current location of the planet and points to its longitude of perihelion. In the case of a blobby eccentric ring, numerical modeling can potentially reveal these parameters.

We thank Tommy Grav, Sean Moran, and Mike Lecar for helpful discussions. This work was performed in part under contract with the Jet Propulsion Laboratory (JPL) through the Michelson Fellowship program funded by NASA as an element of the Planet Finder Program. JPL is managed for NASA by the California Institute of Technology.

REFERENCES

Augereau, J. C., Nelson, R. P., Lagrange, A. M., Papaloizou, J. C. B., & Mouillet, D. 2001, A&A, 370, 447
Banaszkiewicz, M., Fahr, H. J., & Scherer, K. 1994, Icarus, 107, 358
Beauge, C., & Ferraz-Mello, S. 1994, Icarus, 110, 239
Brouwer, D., & Clemence, G. M. 1961, Methods of Celestial Mechanics (New York: Academic Press)
Burns, J. A., Lamy, P., & Soter, S. 1979, Icarus, 40, 1
Burrows, C. J., et al. 1995, BAAS, 187, 32.05
Dermott, S. F., Jayaraman, S., Xu, Y. L., Gustafson, B. Å. S., & Liou, J.-C. 1994, Nature, 369, 719
Dermott, S. F., Nicholson, P. D., Burns, J. A., & Houck, J. R. 1985, in Properties and Interactions of Interplanetary Dust, ed. R. H. Giese & P. Lamy (Dordrecht: Reidel), 395
Duncan, M., Quinn, T., & Tremaine, S. 1989, Icarus, 82, 402
Fixsen, D. J., & Dwek, E. 2002, ApJ, 578, 1009
Gold, T. 1975, Icarus, 25, 489
Greaves, J. S., et al. 1998, ApJ, 506, L133
Greenberg, R. 1978, Icarus, 33, 62
Grun, E., Zook, H. A., Fechtig, H., & Giese, R. H. 1985, Icarus, 62, 244
Hauser, M. G., et al. 1984, ApJ, 278, L15
Holland, W. S., et al. 1998, Nature, 392, 788
———. 2003, ApJ, 582, 1141
Jackson, A. A., & Zook, H. A. 1989, Nature, 337, 629
Koerner, D. W., Sargent, A. I., & Ostroff, N. A. 2001, ApJ, 560, L181
Kuchner, M. J., & Holman, M. 2001, DPS Meeting, 34, 42.08
Kuchner, M. J., Reach, W. T., & Brown, M. E. 2000, Icarus, 145, 44
Lazzaro, D., Sicardy, B., Roques, F., & Greenberg, R. 1994, Icarus, 108, 59
Lecavelier Des Etangs, A., Scholl, H., Roques, F., Sicardy, B., & Vidal-Madjar, A. 1996, Icarus, 123, 168
Liou, J.-C., & Zook, H. A. 1997, Icarus, 128, 354
———. 1999, AJ, 118, 580
Marcy, G. W., & Butler, R. P. 2000, PASP, 112, 137
Marzari, F., & Vanzani, V. 1994, A&A, 283, 275
Murray, C. D., & Dermott, S. F. 1999, Solar System Dynamics (New York: Cambridge Univ. Press)
Ozernoy, L. M., Gorkavyi, N. N., Mather, J. C., & Taidakova, T. A. 2000, ApJ, 537, L147
Quillen, A. C., & Thorndike, S. 2002, ApJ, 578, L149
Reach, W. T. 1991, ApJ, 369, 529
Reach, W. T., et al. 1995, Nature, 374, 521
Robertson, H. P. 1937, MNRAS, 97, 423
Roques, F., Scholl, H., Sicardy, B., & Smith, B. A. 1994, Icarus, 108, 37
Schneider, G., et al. 1999, ApJ, 513, L127
Sicardy, B., Beauge, C., Ferraz-Mello, S., Lazzaro, D., & Roques, F. 1993, Celest. Mech. Dyn. Astron., 57, 373
Weidenschilling, S. J., & Jackson, A. A. 1993, Icarus, 104, 244
Wilner, D. J., Holman, M. J., Kuchner, M. J., & Ho, P. T. P. 2002, ApJ, 569, L115
Wisdom, J. 1980, AJ, 85, 1122
———. 1983, Icarus, 56, 51
Wyatt, M. C., & Dent, W. R. F. 2002, MNRAS, 334, 589
Wyatt, M. C., Dermott, S. F., Telesco, C. M., Fisher, R. S., Grogan, K., Holmes, E. K., & Piña, R. K. 1999, ApJ, 527, 918
Wyatt, S. P., & Whipple, F. L. 1950, ApJ, 111, 134